Human Body Model Based Inertial Measurement of Sit-to-Stand Motion Kinematics

JOSIP MUSIĆ[a], ROMAN KAMNIK[b], VLASTA ZANCHI[a], MARKO MUNIH[b]
[a]Faculty of Electrical Engineering, Mechanical Engineering and Naval Architecture
University of Split
Ruđera Boškovića bb, 21000 Split
CROATIA
[b]Faculty of Electrical Engineering
University of Ljubljana
Tržaška 25, 1000 Ljubljana
SLOVENIA
jmusic@fesb.hr

Abstract: - In the paper a method for measuring kinematics of sit-to-stand motion using inertial sensors and human body model is presented. The proposed method fuses data from inertial sensors and data from three-segment human body model using Extended Kalman filtering technique and in this way alleviates some of the drawbacks associated with inertial sensors. Dynamic human body model is constructed based on principles of Lagrangian dynamics and incorporates shank, thigh and HAT (Head-Arms-Trunk) segments. The moments required in obtained model equations (ankle, knee and hip moments) are calculated based on the EKF last best estimate and Newton-Euler inverse dynamic approach. Outputs from the EKF are segment angles (orientations), angular rates of change (angular velocities) and angular accelerations. The performance of the method is verified by the measurements acquired with Optotrak optical motion analysis system. Obtained results are presented and discussed.

Key-Words: - **inertial sensors, human dynamic body model, Kalman filter, standing-up**

1 Introduction

Microelectromechanical (MEMS) inertial sensors have become widely available over the last few years [1]. Their small size and low cost have made them attractive for wide range of applications in different research areas: robotics [2], navigation and attitude-control systems [3, 4], man-machine interfaces, virtual reality, analysis of human motion [5, 6, 7] etc.

When used in human motion analysis these sensors have some advantages over more sophisticated motion analysis systems commonly used today like Optotrak – Northern Digital Inc. or Vicon - Vicon Motion Systems: a) they are lightweight and portable (DC power supply), b) they don't require complicated and time consuming setting up procedures, c) they are unobtrusive since they don't constrain user in motion, d) they can be used for measurements in subject's natural environment (e.g. subject's home) and e) they are less expensive.

Despite their advantages inertial sensors also have their share of drawbacks [5, 6, 8, 9]. The dynamic and gravitational component in accelerometer output signal can't easily be distinguished during movements with higher accelerations and the drift in gyroscope signal results in large integration errors.

Number of inertial sensor applications are available with different approaches to the elimination/ reduction of inertial sensor errors and extraction of relevant data. Moe-Nilssen [8] examined how accelerometers could be used in measurements of human postural stability (as inclinometer) and concluded that transformation from sensor to Earth coordinate frame was beneficial since it increased discrimination power of the system. The method was tested with a healthy subject and a subject with balance disorder and compared to double integration procedure. Good discrimination and good robustness to drift in time were observed for the test examples. This method is an example of approach where inertial sensors are used as stand-alone sensors providing more of qualitative then quantative information.

Luinge et. al. [10] developed Kalman filter algorithm in which the sensor orientation was determined by integration of gyroscope signal. Obtained orientation was split into two components: the tilt and rotation around global vertical axis.

Calculated tilt was compared to the tilt obtained from accelerometer measurements and the difference presented the input to the Kalman filter. The output from Kalman filter was combined with other gyroscope component (rotation around global vertical axis) to produce better orientation estimate. The proposed method was tested on simulated data on a simple test signals with good matching. Authors noted that larger errors can be expected in practical applications. The approach is an example of a method that uses inertial sensor measurements and signal processing algorithms to obtain position and orientation data.

Zhu and Zhou [6] proposed a real-time motion tracking system based on inertial and magnetic sensors. Linear Kalman filter was used for data fusion of different sensor outputs and produced an estimate of segment position and orientation. Authors suggested the application of 15-segment human body model for full human motion tracking, however the implementation was not described in the paper. The proposed method was tested in manual manipulation on horizontal plane and rotation on single-axis rotating table. Testing was also accomplished on actual arm movement tracked by three inertial sensor modules attached to upper trunk and upper and lower arm. Performance of the method was compared to reference values, integration based and accelerometer-magnetometer based approaches. Obtained results demonstrated good matching with reference values and superior performance to other two methods.

Zhou and Hu [11] proposed the development of the system based on commercially available inertial and magnetic modules for kinematic measurements of upper extremities. Recorded data was pre-filtered in order to eliminate high frequency noise and low frequency drift and was followed by anti-aliasing filtering. Transformation of coordinates was performed in order to express data in world coordinate frame in form of quaternions. Kinematic modeling and optimization algorithms were applied to obtain better orientation estimates. Validation was accomplished on experimental data recorded on several daily living activities: reach, drink, eating and arm flexion-extension. CODA marker kinematic measurement system was used for simultaneous reference measurements. Authors concluded that the proposed method was precise and stable in arm orientation estimation but suggested additional testing in home environment.

Inertial/magnetic sensor based methods yield good results but introduce additional restrictions on measurement environment [5, 6, 12]. These restrictions can not easily be fulfilled in average ambulatory setting and presence of ferrous materials and devices that emit electromagnetic field can potentially result in faulty magnetometer readings. More recently, an effort has been made toward the development of filtering techniques for reduction of magnetic disturbance effects [12], by implementation of complementary Kalman filter based on error models for every sensor (most importantly magnetometer). From data fusion the information about gyroscope, accelerometer and magnetometer offsets were obtained which were used for in-use sensor re-calibration. Experimental validation with good tracking was achieved by placing an iron cylinder near the sensor and by comparing the orientation estimates with Vicon reference measurements. However additional testing is required since experimental measurements were performed in controlled and limited conditions.

In our proposal we assume that magnetometers can in certain applications (e.g. robot assisted sit-to-stand motion) be substituted by dynamic human body model. In this approach, which we named "Model Based Inertial Sensing", data acquired from inertial sensors and data from dynamic human body model are fused using Extended Kalman Filter (EKF) alleviating some of the drawbacks associated with magnetometers while maintaining required level of accuracy. The paper is structured as follows. In Section 2 construction of dynamic human body model is presented. Next, the accelerometer signal decomposition is explained and EKF design outlined. In Section 3 experimental validation procedure is presented followed by presentation of the results. Finally in Section 4, after the discussion, conclusions are drawn and guidelines for improvement of the method are suggested.

2 Materials and methods

2.1 Dynamic human body model

The proposed method is based on dynamic human body model corresponding to simplified model of human subject performing standing-up motion viewed in sagittal plane. The model consists of three rigid segments corresponding to shank, thigh and HAT (Head-Arms-Trunk) as depicted in Figure 1. In the figure the following notation is used

Θ_i - angle of the *i*-th segment in respect to horizontal (*y*) axis,
m_i - mass of the *i*-th segment,
l_i - length of the *i*-th segment,
c_i - distance of the *i*-th segment Center of Mass

(CoM) from distal joint,
i = 1, 2, 3.

Anthropometric data i.e. segment masses, lengths and CoM positions are obtained from the literature [13].

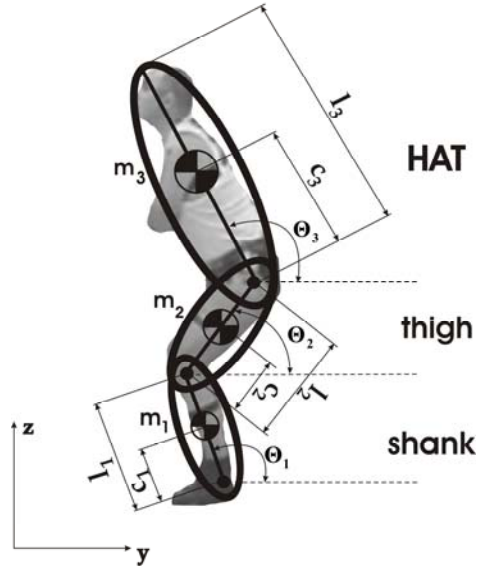

Fig. 1 – Three segment dynamic human body model

During the modeling phase the following simplifications were introduced: a) human body motion is restricted to the sagittal plane, b) symmetry of sit-to-stand motion in respect to sagittal plane is assumed [14], c) joints are assumed to be ideal with no friction during rotation, d) segments are assumed to be rigid bodies with their masses contained at CoM, e) the model is in contact with environment only by shank segment (i.e. ankle joint).

Mathematical description of the proposed three-segment dynamic human body model was obtained using principles of Lagrangian dynamics [15]. These principles enable derivation of dynamic equations of motion of a complex system using a set of simple procedures which as a result produce system of differential equations. In general, number of differential equations equals the number of generalized coordinates (sometimes called Lagrangian coordinates) i.e. the number of degrees of freedom of the system. A great variety of coordinates may be used, depending on parameters of interest. In the modeling phase several sets of generalized coordinates were tested. Finally, a set of generalized coordinates defined as segment angles Θ_1, Θ_2 and Θ_3 was chosen. In the set each angle was defined as the angle between the corresponding segment and horizontal (*y*) axis in the counter-clockwise direction (see Figure 1). This angle definition produced mathematical description of the model with lowest complexity (as compared to other angle definitions that were tested) thus reducing subsequent computational cost.

For each degree of freedom the Lagrangian equation is written:

$$\frac{d}{dt}\left(\frac{\partial K}{\partial \dot{\Theta}_i}\right) - \frac{\partial K}{\partial \Theta_i} + \frac{\partial V}{\partial \Theta_i} = T_i \qquad (1)$$

where:
K – is kinetic energy of the system,
V – is potential energy of the system, and
T_i – is the sum of generalized forces/moments applied on the *i*-th segment.

Figure 2 depicts model joints with corresponding joint moment notation.

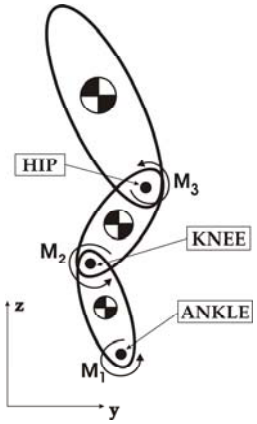

Fig. 2 – Model joints and notation of corresponding joint moments

Using (1) and notations from Figure 1 and Figure 2, non-linear, coupled differential equations of motion for shank (2), thigh (3) and HAT (4) are derived. From (2)-(4) segment angles (orientations), angular velocities and angular accelerations can be calculated. Since the intended application of the proposed method is in rehabilitation (robot assisted standing-up [16]), segment orientations are considered to be most important kinematic parameters from which all other kinematic parameters can be obtained.

2.2 Accelerometer signal analysis

The output of inertial accelerometer consists of two components, dynamic and the gravitational [7, 8, 9]. The dynamic component represents true acceleration of system to which the accelerometer is attached to, while the gravitational component represents Earth gravity. Figure 3 presents characteristic sensor orientations in respect to Earth surface. As it can be seen from the figure, the problems arise when sensor motion is not aligned with its sensitive axis, in which case the true

$$\ddot{\Theta}_1(m_1c_1^2+m_2l_1^2+m_3l_1^2+I_{x1})+\ddot{\Theta}_2\cos(\Theta_1-\Theta_2)(m_2l_1c_2+m_3l_1l_2)+\ddot{\Theta}_3\cos(\Theta_1-\Theta_3)m_3l_1c_3+$$
$$\dot{\Theta}_2^2\sin(\Theta_1-\Theta_2)(m_2l_1c_2+m_3l_1l_2)+\dot{\Theta}_3^2\sin(\Theta_1-\Theta_3)m_3l_1c_3+g(m_1c_1+m_2l_1+m_3l_1)\cos\Theta_1=M_1-M_2 \quad (2)$$

$$\ddot{\Theta}_2(m_2c_2^2+m_3l_2^2+I_{x2})+\ddot{\Theta}_1\cos(\Theta_1-\Theta_2)(m_2l_1c_2+m_3l_1l_2)+\ddot{\Theta}_3\cos(\Theta_2-\Theta_3)m_3l_2c_3-$$
$$\dot{\Theta}_1^2\sin(\Theta_1-\Theta_2)(m_2l_1c_2+m_3l_1l_2)+\dot{\Theta}_3^2\sin(\Theta_2-\Theta_3)m_3l_2c_3+g(m_2c_2+m_3l_2)\cos\Theta_2=M_2-M_3 \quad (3)$$

$$\ddot{\Theta}_3(m_3c_3^2+I_{x3})+\ddot{\Theta}_1\cos(\Theta_1-\Theta_3)m_3l_1c_3+\ddot{\Theta}_2\cos(\Theta_2-\Theta_3)m_3l_2c_3-$$
$$\dot{\Theta}_1^2\sin(\Theta_1-\Theta_3)m_3l_1c_3-\dot{\Theta}_2^2\sin(\Theta_2-\Theta_3)m_3l_2c_3+gm_3c_3\cos\Theta_3=M_3 \quad (4)$$

acceleration is projected onto accelerometer sensitive axis along with gravitational component. If it is assumed that the motion of accelerometer has significantly lower acceleration than the Earth gravity constant, the angle between the two components of the output signal can be calculated [8].

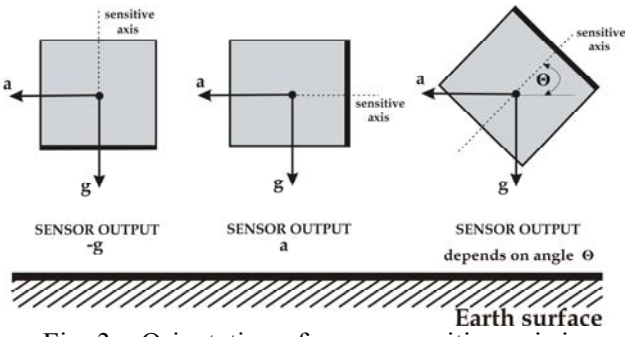

Fig. 3 – Orientation of sensor sensitive axis in respect to Earth surface and the sensor output

The same can not be accomplished when the amplitude of true sensor acceleration has values close to Earth gravity constant, thus explicit knowledge of sensor orientation is required. Since the accelerations expressed in reference coordinate frame (vertical-horizontal frame in respect to Earth surface) are of interest, processing of the accelerometer output is required [8, 9].

In order to obtain accelerations along z_{REF} and y_{REF}, the decomposition of accelerometer signal to its main components representing projections of dynamic and gravitational acceleration to sensor sensitive axis must be accomplished. These projections are then projected back onto the reference frame and true vertical and horizontal accelerations are calculated. For this, the angle between sensor coordinate frame and reference coordinate frame (i.e. sensor orientation) needs to be known. The sensor orientation is defined as the angle between the *z* sensor axis and *y* axis of reference coordinate frame as is shown in Figure 4. This angle definition was chosen because of compatibility with angle definition used in dynamic human body model. The actual sensor accelerations in vertical and horizontal directions are derived using (5) and (6).

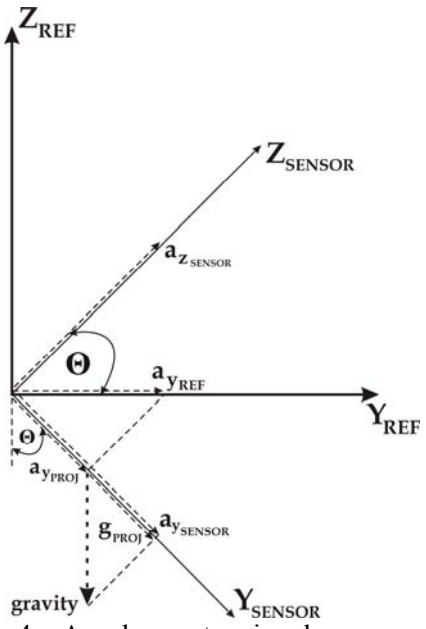

Fig. 4 – Accelerometer signal components

$$a_{y_{SENSOR}}=a_{y_{REF}}\sin\Theta+g\cos\Theta \quad (5)$$
$$a_{z_{SENSOR}}=a_{z_{REF}}\sin\Theta+g\sin\Theta \quad (6)$$

The accelerometer signal decomposition for *y* component is graphically depicted in Figure 4. Because of the nature of the inertial sensing, direction of the dynamic acceleration output is opposite to actual direction of the motion and is taken into account in later calculations.

The sensor angle (sensor orientation) Θ is in the proposed method available as a system state of the Extended Kalman filter (EKF).

2.3 Extended Kalman Filter architecture

Kalman filtering is a technique widely used in multisignal integration tasks [4, 6, 10, 12, 17, 18]. In essence it filters out the noise from the data by combining multiple data sources in a recursive

$$\begin{bmatrix} h_1 \\ h_2 \\ h_3 \\ h_4 \\ h_5 \\ h_6 \\ h_7 \\ h_8 \\ h_9 \\ h_{10} \\ h_{11} \\ h_{12} \end{bmatrix} = \begin{bmatrix} \dot{\Theta}_1 \\ \dot{\Theta}_2 \\ \dot{\Theta}_3 \\ (-c_1\ddot{\Theta}_1 \sin\Theta_1 - c_1\dot{\Theta}_1^2 \cos\Theta_1)\sin\Theta_1 - g\cos\Theta_1 \\ -(c_1\ddot{\Theta}_1 \cos\Theta_1 - c_1\dot{\Theta}_1^2 \sin\Theta_1)\sin\Theta_1 - g\sin\Theta_1 \\ (-l_1\ddot{\Theta}_1 \sin\Theta_1 - l_1\dot{\Theta}_1^2 \cos\Theta_1 - c_2\ddot{\Theta}_2 \sin\Theta_2 - c_2\dot{\Theta}_2^2 \cos\Theta_2)\sin\Theta_2 - g\cos\Theta_2 \\ -(l_1\ddot{\Theta}_1 \cos\Theta_1 - l_1\dot{\Theta}_1^2 \sin\Theta_1 + c_2\ddot{\Theta}_2 \cos\Theta_2 - c_2\dot{\Theta}_2^2 \sin\Theta_2)\sin\Theta_2 - g\sin\Theta_2 \\ (-l_1\ddot{\Theta}_1 \sin\Theta_1 - l_1\dot{\Theta}_1^2 \cos\Theta_1 - l_2\ddot{\Theta}_2 \sin\Theta_2 - l_2\dot{\Theta}_2^2 \cos\Theta_2 - c_3\ddot{\Theta}_3 \sin\Theta_3 - c_3\dot{\Theta}_3^2 \cos\Theta_3)\sin\Theta_3 - g\cos\Theta_3 \\ -(l_1\ddot{\Theta}_1 \cos\Theta_1 - l_1\dot{\Theta}_1^2 \sin\Theta_1 + l_2\ddot{\Theta}_2 \cos\Theta_2 - l_2\dot{\Theta}_2^2 \sin\Theta_2 + c_3\ddot{\Theta}_3 \cos\Theta_3 - c_3\dot{\Theta}_3^2 \sin\Theta_3)\sin\Theta_1 - g\sin\Theta_1 \\ M_2 + K_{11}\ddot{\Theta}_1 + K_{12}\ddot{\Theta}_2 \cos(\Theta_1 - \Theta_2) + K_{13}\ddot{\Theta}_3 \cos(\Theta_1 - \Theta_3) + K_{14}\dot{\Theta}_2^2 \sin(\Theta_1 - \Theta_2) + K_{15}\dot{\Theta}_3^2 \sin(\Theta_1 - \Theta_3) + K_{16}\cos\Theta_1 \\ M_3 + K_{22}\ddot{\Theta}_2 + K_{21}\ddot{\Theta}_1 \cos(\Theta_1 - \Theta_2) + K_{23}\ddot{\Theta}_3 \cos(\Theta_2 - \Theta_3) - K_{24}\dot{\Theta}_1^2 \sin(\Theta_1 - \Theta_2) + K_{25}\dot{\Theta}_3^2 \sin(\Theta_2 - \Theta_3) + K_{26}\cos\Theta_2 \\ K_{33}\ddot{\Theta}_3 + K_{31}\ddot{\Theta}_1 \cos(\Theta_1 - \Theta_3) + K_{32}\ddot{\Theta}_2 \cos(\Theta_2 - \Theta_3) - K_{34}\dot{\Theta}_1^2 \sin(\Theta_1 - \Theta_3) - K_{35}\dot{\Theta}_2^2 \sin(\Theta_2 - \Theta_3) + K_{36}\cos\Theta_3 \end{bmatrix} \quad (10)$$

manner and for the operation needs only data from the current time instance as well as from the previous one. This makes the Kalman filter computationally efficient and suitable for real time applications. Due to non-linearities present in three-segment dynamic human body model a variant of the filter, the EKF, had to be used. The EKF performs linearization of the system at every time instance and then uses the linearized model for its operation [19]. In the proposed method the EKF is employed for fusion of the acquired inertial data and data from dynamic human body model. In the proposed EKF the system is described by
the system equation

$$\hat{\mathbf{x}}_k^- = \mathbf{A} \cdot \hat{\mathbf{x}}_{k-1}^+ + \mathbf{w} \quad (7)$$

and the measurement equation

$$\mathbf{z}_k = \mathbf{h}(\mathbf{x}_k, \mathbf{v}_k) \quad (8)$$

In (7) **x** denotes the state vector, **A** the transition matrix and **w** the white process noise. In (8) **h** represents the (non-linear) measurement vector and **v** is the white measurement noise. In the Kalman filter algorithm an assumption is made that noises **v** and **w** are Gaussian distributed, have zero mean and are uncorrelated [19].
During the EKF design, several filter structures were tested and the structure with lowest computational cost and highest achieved accuracy was chosen and is represented by (9) and (10).

$$\begin{bmatrix} \dot{\Theta}_1 \\ \ddot{\Theta}_1 \\ \dddot{\Theta}_1 \\ \dot{\Theta}_2 \\ \ddot{\Theta}_2 \\ \dddot{\Theta}_2 \\ \dot{\Theta}_3 \\ \ddot{\Theta}_3 \\ \dddot{\Theta}_3 \end{bmatrix} = \begin{bmatrix} 0 & 1 & 0 & 0 & 0 & 0 & 0 & 0 & 0 \\ 0 & 0 & 1 & 0 & 0 & 0 & 0 & 0 & 0 \\ 0 & 0 & 0 & 0 & 0 & 0 & 0 & 0 & 0 \\ 0 & 0 & 0 & 0 & 1 & 0 & 0 & 0 & 0 \\ 0 & 0 & 0 & 0 & 0 & 1 & 0 & 0 & 0 \\ 0 & 0 & 0 & 0 & 0 & 0 & 0 & 0 & 0 \\ 0 & 0 & 0 & 0 & 0 & 0 & 0 & 1 & 0 \\ 0 & 0 & 0 & 0 & 0 & 0 & 0 & 0 & 1 \\ 0 & 0 & 0 & 0 & 0 & 0 & 0 & 0 & 0 \end{bmatrix} \cdot \begin{bmatrix} \Theta_1 \\ \dot{\Theta}_1 \\ \ddot{\Theta}_1 \\ \Theta_2 \\ \dot{\Theta}_2 \\ \ddot{\Theta}_2 \\ \Theta_3 \\ \dot{\Theta}_3 \\ \ddot{\Theta}_3 \end{bmatrix} \quad (9)$$

In the measurement equation (10) the parameters are defined as follows:

$$K_{11} = m_1 c_1^2 + m_2 l_1^2 + m_3 l_1^2 + I_{x1}$$
$$K_{12} = K_{14} = K_{21} = K_{24} = m_2 l_1 c_2 + m_3 l_1 l_2$$
$$K_{13} = K_{15} = m_3 l_1 c_3$$
$$K_{16} = g(m_1 c_1 + m_2 l_1 + m_3 l_1)$$
$$K_{22} = m_2 c_2^2 + m_3 l_2^2 + I_{x2}$$
$$K_{23} = K_{25} = K_{32} = K_{35} = m_3 l_2 c_3$$
$$K_{26} = g(m_2 c_2 + m_3 l_2)$$
$$K_{31} = K_{34} = m_3 l_1 c_3$$
$$K_{33} = m_3 c_3^2 + I_{x3}$$
$$K_{36} = m_3 g c_3$$

The measurement vector comprises two types of data: directly and indirectly measurable data. Directly measurable data is acquired via inertial sensors measurements and includes the following measurement vector components

$$\dot{\Theta}_1 \equiv h_1 \qquad a_{y2} \equiv h_6$$
$$\dot{\Theta}_2 \equiv h_2 \qquad a_{z2} \equiv h_7$$
$$\dot{\Theta}_3 \equiv h_3 \qquad a_{y3} \equiv h_8$$
$$a_{y1} \equiv h_4 \qquad a_{z3} \equiv h_9$$
$$a_{z1} \equiv h_5$$

where: a_{yi} – acceleration of the *i*-th segment CoM in the direction of reference frame *y* axis (horizontal)
a_{zi} – acceleration of the *i*-th segment CoM in the direction of reference frame *z* axis (horizontal)

Using kinematic equations, a term linking segment linear accelerations to used generalized coordinates is derived as it can be seen in (10).
Indirectly measurable data is acquired via Newton-Euler inverse dynamic approach using the EKF last best estimate, force plate measurements and anthropometric data. It includes the following measurement vector components expressed in terms

of equations of the proposed dynamic human body model

$$M_1 \equiv h_{10}$$
$$M_2 \equiv h_{11}$$
$$M_3 \equiv h_{12}$$

The EKF algorithm was implemented according to [17] and [19] as shown below:
Measurement update is

$$\mathbf{K}_k = \mathbf{P}_k^- \mathbf{H}_k^T (\mathbf{H}_k \mathbf{P}_k^- \mathbf{H}_k^T + \mathbf{R}_k)^{-1} \quad (11)$$

$$\hat{\mathbf{x}}_k = \hat{\mathbf{x}}_k^- + \mathbf{K}(\mathbf{z}_k - \mathbf{h}(\hat{\mathbf{x}}_k^-, 0)) \quad (12)$$

$$\mathbf{P}_k = (\mathbf{I} - \mathbf{K}_k \mathbf{H}_k)\mathbf{P}_k^- \quad (13)$$

and time update is

$$\mathbf{P}_{k+1}^- = \mathbf{A}_k \mathbf{P}_k \mathbf{A}_k^T + \mathbf{Q}_k \quad (14)$$

where: $\hat{\mathbf{x}}_k^-$ - *a priori* state vector estimate,

$\hat{\mathbf{x}}_k$ - *a posteriori* state vector estimate,

$\mathbf{P}_k^-$ – *a priori* estimate error covariance matrix,

$\mathbf{P}_k^+$ – *a posteriori* estimate error covariance matrix,

$\mathbf{K}_k$ – Kalman gain,

$\mathbf{H}_k = \frac{\partial h_i}{\partial x_j}(\mathbf{x}_k, 0)$ – the Jacobian matrix of partial derivates of $\mathbf{h}()$ with respect to $\mathbf{x}$ i.e. linearized measurement vector around the EKF last best estimate,

$\mathbf{R}_k$ – measurement noise covariance matrix,

$\mathbf{Q}_k$ – process noise covariance matrix.

Equations (7), (8) and (11)-(14) form the complete set of equations for the EKF algorithm used in the proposed method. The EKF initial system state estimates were set to true system state in all experimental runs.

3 Experimental validation

3.1 Experimental setup and procedure

The proposed method was verified on a healthy subject performing four sit-to-stand trials with normal/self-selected speed. The Optotrak 3010 optical motion analysis system was used for measurements of kinematic parameters of standing-up. Inertial sensor specific noise were later added to the measured signals in order to obtain EKF input data. Measurement setup presented in Figure 5 was constructed for the purpose of experimental measurements. Set of linear infrared cameras was positioned parallel to the subject's sagittal plane in a way that all infrared (IR) markers are in its field of view at all times. Four IR markers were attached to subject's skin at key anatomical positions: ankle, knee, hip and shoulder joints. Trajectories of the four markers (with 50Hz sampling rate) fully describe subject standing-up motion and correspond to trajectories of segment endpoints in the three segment dynamic human body model.

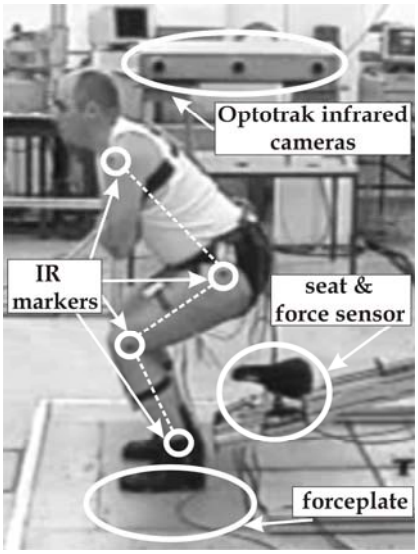

Fig 5. – Measurement setup

Subject was standing on AMTI OR6-5-1 force plate which measured ground reaction forces during standing up. These forces (and moments) are used for calculation of joint moments which are part of the EKF state vector. Optionally, the force plate can in ambulatory settings be substituted by shoe insole with force sensor [20]. The seat was mounted on top of the multidimensional force sensor (model 40E15 from JR3 Inc.) to enable detection of seat-off moment. The knowledge of seat-off moment is of importance because the proposed three segment dynamic human body model is valid only at those times when there is no subject-seat interaction. The seat-off moment was detected as the moment when the amplitude of vertical force component felt beneath the 5% of the value it had when the subject was sitting quietly. However, in ambulatory setting a simple On/Off switch would be sufficient for seat contact detection. Seat/force sensor structure was mounted on the end of leaver like structure which ensured unobstructed execution of sit-to-stand maneuver.

Table 1 –Test subject data

Initials	Gender	Age	Height	Weight
JK	M	23	1.77 m	77 kg

The measurement procedure during the sit-to-stand measurements was as follows. The test subject was weighted and his height measured in order to determine input data for anthropometric tables (see Table 1). The subject did not suffer of any medical conditions which would constrain normal accomplishment of standing-up motion.
Before the recorded measurements subject accomplished three sit-to-stand trials in order to get familiar with measurement equipment and measurement environment. Then he prepared in initial position on the seat, and waited for the operator to start the recording of data and to begin with rising. The operator stopped the measurement when the test subject was in standing position for about 2 seconds. After each measurement the subject returned to initial position for the next measurement trial. Recorded positional coordinates of the markers with respect to reference coordinate frame were numerically differentiated to obtain velocities and accelerations of each segment. Recorded data was also used for calculation of segment orientations which were later used as reference measurements. Velocity and acceleration signals were then low-pass filtered with Butterworth filter with 5 Hz cut-off frequency in order to eliminate noise components. The same filtering algorithm was applied on force sensor measurements. The whole procedure introduced additional numerical error to the EKF input signals. Finally, inertial sensor specific noise was added to angular velocity and linear acceleration signals which were presented to the EKF as part of the measurement vector. The data flow in the experimental validation is depicted in Figure 6.

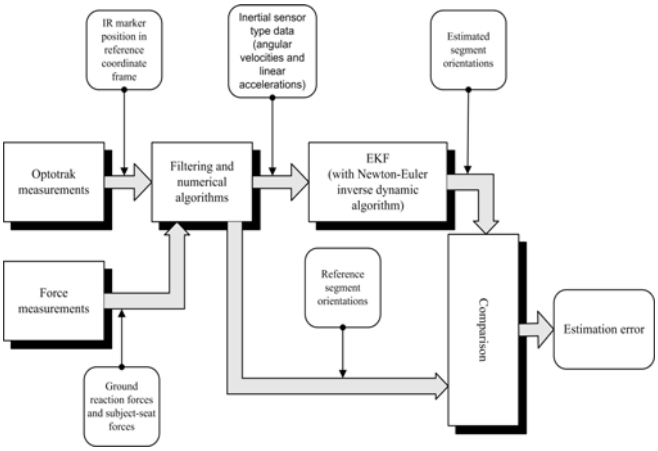

Fig 6. – Experimental validation data flow chart

3.2 Experimental results

The obtained results of joint angle estimates compared to the reference measurements for one measurement trial are presented in Figure 7, while Figure 8 depicts root mean square error (RMSE) values for each of angle estimates.
Figure 9 presents average value of segment angles over all four measurement trials with standard deviation defined for every 10% of time required for successful standing up motion (with the beginning at seat-off moment). Figure 10 depicts RMSE for shank, thigh and HAT segment for all four measurement trials.

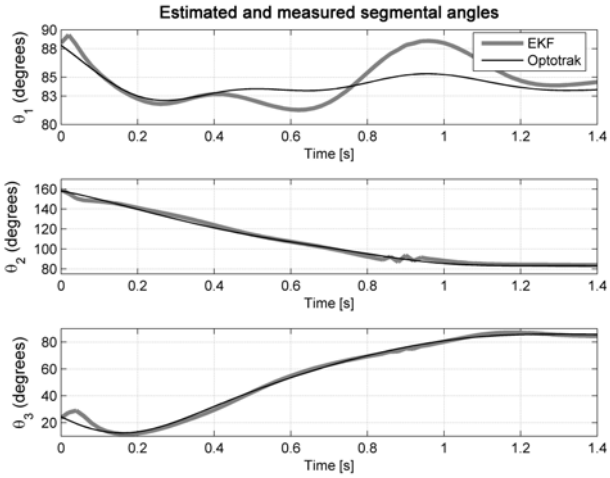

Fig 7. – Comparison of reference measurements and estimation

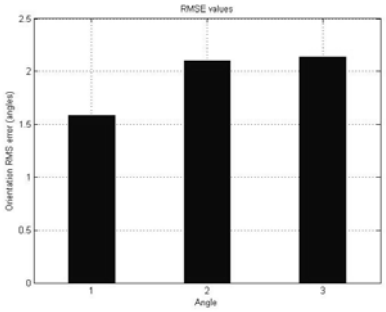

Fig 8. – RMSE values

4. Discussion and conclusion

Obtained results show good tracking capability for all three estimated segment angles. The average estimation error (RMSE) over four measurements is 3.75° for the shank, 2.41° for the thigh and 4.48° for the HAT segment. Obtained estimation error is comparable to similar methods which do not use magnetometers as additional sensor. However, it is less accurate then methods that use magnetometers but it is not sensitive to presence of ferrous objects or devices that emit electromagnetic field during operation.
Estimated shank angle has certain amount of oscillations for every measurement trial. This was

attributed to selected filter parameters (matrices **R** and **Q**) and to Newton-Euler inverse dynamic approach. Filter parameter selection i.e. filter tuning was done manually and selected parameters were used for all four measurement runs. This proved to be time consuming and there was no guarantee that chosen parameters were the optimal. Thus, introduction of Adaptive Extended Kalman Filter is planned (AEKF). The AEKF would be implemented similar as in [3] and would change parameters **R** and **Q** depending on current system dynamics since from Figure 9 it can be seen that standard deviation of angle estimation is higher during transition phase (app. from 0.4-1 s). In this way we believe better filter performance could be achieved and previously mentioned oscillations reduced.

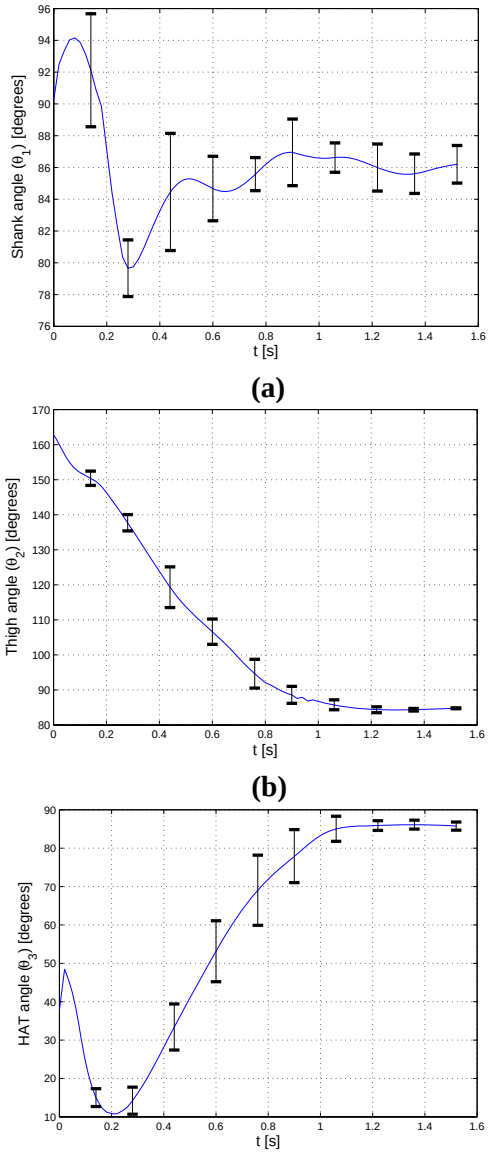

Fig. 9 – Average value for estimated segment angles: a) shank, b) thigh and c) HAT

In general, HAT angle estimation error is the largest and this is attributed to the fact that equations describing its motion have more complex form in respect to other segments. Estimated thigh angle error has the lowest RMSE value, but we assume that this will change when AEKF is applied since shank motion is described by kinematic equations of lower complexity and by selection of optimal filter parameters it should achieve the lowest RMSE value (as in case of Measurement 1 in Figure 10).

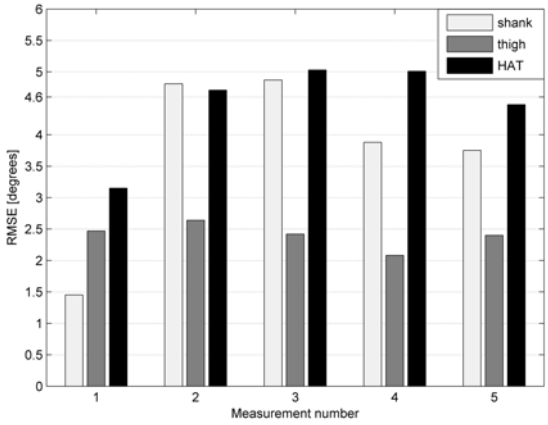

Fig. 10 – RMSE values for all measurement trials

Further accuracy improvements could be accomplished if three-segment dynamic human body model is augmented to include some phenomena that were neglected during modeling phase as are joint friction and restriction of movement to sagittal plane. Addition of several more body segments (e.g. head, lower and upper trunk) could also be beneficial in terms of accuracy but mathematical complexity of the model and associated kinematic equations would increase significantly, thus further analysis is required.

The presented approach and its results are the first stage in development phase of low cost inertial sensor based kinematic measurement system. The system is aimed to be used in conjunction with robot assistive devices (e.g. for standing-up support). Achieved experimental results demonstrate feasibility of the proposed "Model Based Inertial Sensing" method, with good tracking for all segment angles. Using numerical algorithms segment angular velocities and angular accelerations can be calculated. In this way complete set of kinematic parameters of the human standing-up motion is derived. In future research the method will be tested using actual inertial sensor measurements on group of healthy and impaired subjects with simultaneous measurements with commercially available inertial/magnetic sensors for comparison. The influence of the standing-up speed on method

performance will also be examined Finally, inclusion of the proposed method in control scheme of robot rehabilitation device for standing-up support as kinematic measurement system and its testing is planned.

References:

[1] R. Bogue, MEMS sensors: past, present and future, *Sensor Review,* Vol. 27, No. 1, 2007, pp. 7-13

[2] P. Corke, J. Lobo, J. Dias, An introduction to inertial and visual sensing, *The International Journal of Robotics Research*, Vol. 26, No. 6, 2007, pp. 519-535

[3] D. Jurman, M. Jankovec, R. Kamnik, M. Topič, Calibration and data fusion solution for the miniature attitude and heading reference system, *Sensors and Actuators A*, Vol. 138, No. 2, 2007, pp. 411-420

[4] J. Jackson, D. Callahan, P. Wang, A preliminary examination of inertial navigation using accelerometers, WSEAS *Transactions on Circuits and Systems*, Vol. 5, No. 12, 2006, pp. 1789-1795

[5] D. Roetenberg, P. J. Slycke, P. H. Veltink, Ambulatory position and orientation tracking fusing magnetic and inertial sensing, *IEEE Transactions on Biomedical Engineering*, Vol. 54, No. 5, 2007, pp. 883-890

[6] R. Zhu, Z. Zhou, A real-time articulated human motion tracking using tri-axis inertial/magnetic sensor package, *IEEE Transactions on Neural Systems and Rehabilitation Engineering*, Vol. 12, No. 2, 2004, pp. 295-302

[7] R. Kamnik, J. Musić, H. Burger, M. Munih, T. Bajd, Design of inertial motion sensors and its usage in biomechanical analysis, *In proceedings of EPE'06*, 2006, pp. 511-516

[8] R. Moe-Nilssen, A new method for evaluating motor control in gait under real-life environmental conditions. Part 1: The instrument, *Clinical Biomechanics*, Vol. 13, 1998, pp. 320-327

[9] D. Giansanti, V. Macellari, G. Maccioni, A. Cappozzo, Is it feasible to reconstruct body segment 3-D position and orientation using accelerometer data?, *IEEE Transactions on Biomedical Engineering*, Vol. 50, No. 4, 2003, pp. 476-483

[10] H. Luinge, P. Veltink, C. Baten, Estimating orientation with gyroscope and accelerometers, *Technology and Healthcare*, Vol. 7, No. 6, 1999, pp. 455-459

[11] H. Zhou, H. Hu, Inertial sensor for motion detection of human upper limbs, *Sensor Review*, Vol. 27, No. 2, 2007, pp. 151-158

[12] D. Roetenberg, H. Luinge, C. Baten, P. Veltink, Compesation of magnetic disturbances improves inertial and magnetic sensing of human body segment orientation, *IEEE Transactions on Neural Systems and Rehabilitation Engineering*, Vol. 13, No. 3, 2005, pp. 395-405

[13] P. D. Leva, Adjustment to Zatsiorksy-Seluyanov's segment inertia parameters, *Journal of Biomechanics,* Vol. 29, No. 9, 1996, pp. 1223-1230

[14] T. Lundin, M. Grabiner, D. Jahnigen, On the assumption of bilateral lower extremity joint moment symmetry during the sit-to-stand tasks, *Journal of Biomechanics*, Vol. 28, No. 1, 1995, pp. 109-112

[15] D. A. Winter, *Biomechanics and motor control of human movement*, Wiley-Interscience, New York, USA, 1990

[16] R. Kamnik, T. Bajd, Human Voluntary activity integration in the control of a standing-up rehabilitation robot: A simulation study, *Medical Engineering and Physics*, Vol. 29, No. 9, 2007, pp. 1019-1029

[17] R. Kamnik, F. Boettiger, K. Hunt, Roll dynamics and lateral load transfer estimation in articulated heavy freight vehicles, *Journal of Automobile Engineering,* Vol. 217, Part D, 2003, pp. 985-997

[18] A. Kuzu, S. Bogosyan, Comparison of multisensor fusion techniques for improvement of measurement accuracy with MEMS accelerometers, *In proceedings of 2nd WSEAS International Conference on Applied and Theoretical Mechanics*, 2006, pp. 296-301

[19] G. Welch, G Bishop, *An introduction to the Kalman filter*, Technical Report 95-041, University of North Carolina, 2003

[20] P. Veltink, C. Liedtke, E. Droog, H. van der Kooij, Ambulatory measurement of ground reaction forces, *IEEE Transactions on Neural Systems and Rehabilitation Engineering*, Vol. 13, No. 3, 2005, pp. 423-427